Electro-Optical Imaging Microscopy of Dye-Doped Artificial Lipidic Membranes

Bassam Hajj,[†*] Sophie De Reguardati,[‡] Loïc Hugonin,[‡] Bruno Le Pioufle,[‡] Toshihisa Osaki,[§] Hiroaki Suzuki,[§] Shoji Takeuchi,[§] Halina Mojzisova,[†] Dominique Chauvat,[†] and Joseph Zyss[†]

[†]Laboratoire de Photonique Quantique et Moléculaire, Centre National de la Recherche Scientifique, UMR8537 and [‡]Systèmes et Applications des Technologies de l'Information et de l'Energie, Centre National de la Recherche Scientifique, UMR8029, d'Alembert Institute, Ecole Normale Supérieure de Cachan, Cachan, France; and [§]Center for International Research on Micro Mechatronics, Institute of Industrial Science, University of Tokyo, Tokyo, Japan

ABSTRACT Artificial lipidic bilayers are widely used as a model for the lipid matrix in biological cell membranes. We use the Pockels electro-optical effect to investigate the properties of an artificial lipidic membrane doped with nonlinear molecules in the outer layer. We report here what is believed to be the first electro-optical Pockels signal and image from such a membrane. The electro-optical dephasing distribution within the membrane is imaged and the signal is shown to be linear as a function of the applied voltage. A theoretical analysis taking into account the statistical orientation distribution of the inserted dye molecules allows us to estimate the doped membrane nonlinearity. Ongoing extensions of this work to living cell membranes are discussed.

INTRODUCTION

As the main component of cellular membranes, lipid bilayers play an essential role as a barrier protecting the cell and its intracellular organelles. The cellular membranes also maintain the solute and ion concentration gradients that induce the equilibrium transmembrane potential. In the case of excitable cells, the plasma membrane ensures the propagation of the action potential.

Various experimental techniques have been used in cellular electrophysiology for stimulation and measurement of membrane potentials by use of intracellular electrodes (1,2), which has led to the well-known patch-clamp technique (3). Although these techniques are extremely sensitive and allow recording the electrical activity down to a single ion channel, they lead to cell death and provide the information about the potential only at a single location within one neuron. Optical approaches using light scattering and intrinsic birefringence changes were investigated (4,5). Voltage-sensitive amphiphilic dyes were introduced to enhance the latter effect (6), and were found to display voltage-dependent changes in absorption, dichroism (7), and fluorescence (8,9). Such electrometric dyes bind to the external cell membranes and contain an electron donor-acceptor group leading to electrochromism and a high hyperpolarizability. The membrane depolarization and the subsequent action potential propagation can then be recorded at different points of the cell as a voltage-induced fluorescence variation (10–12), or by nonlinear microscopy techniques, in particular by second-harmonic generation (SHG) (13–15). Voltage-induced SHG is, in fact, a third-order nonlinear process described by an effective rank-four nonlinear susceptibility tensor associated to both quadratic and cubic time-dependent molecular hyperpolarizability tensors. The former is underlying field-induced orientational effects and the latter instantaneous four-wave mixing. Therefore, SHG-based membrane potential measurements monitor the electrically induced changes of hyperpolarizability and/or the alignment of the dye molecules in the bilayer (14,15). A major interest of nonlinear microscopy lies in its intrinsic three-dimensional sectioning capability related to the two-photon excitation step that occurs mainly in the focal volume together with the low photobleaching of out-of-focus molecules. It should be noted, however, that the bleaching may be increased in the focal spot due to the use of pulsed femtosecond lasers. Indeed, a high power laser source, such as a Ti:Sapphire femtosecond laser oscillator, is needed in view of the higher order (e.g., third-order with underlying rank four tensors) of the invoked phenomena. Lower-order effects (such as second-order) would be preferable in some ways, to allow for the possibility of using lower power sources, and eventually, continuous-wave lasers, such as low cost He-Ne or semiconductor lasers. In this perspective, one can take advantage of the noncentrosymmetric organization of the dye molecules when inserted exclusively into the external membrane layer. This is a well-known prerequisite toward quadratic nonlinear optical processes such as SHG as well as the related electro-optical Pockels effect (16). The Pockels effect is a variation of the index of refraction Δn induced by a quasistatic applied electric field. When probed by a laser beam, Δn induces an optical phase shift that can be detected with an interferometric setup. Because the Pockels effect is a nonresonant process, it preserves the integrity of the sample, and because it is linear in the optical electric field strength, it can be measured using a low-power continuous-wave laser—avoiding the use of costly and cumbersome high-power, short-pulse lasers.

In this work, we present an original electro-optical microscopy study of the variation of membrane potential in model

Submitted April 2, 2009, and accepted for publication August 17, 2009.

*Correspondence: bassamhajj85@hotmail.com

Editor: Joshua Zimmerberg.

0006-3495/09/12/2913/9 $2.00

doi: 10.1016/j.bpj.2009.08.055

lipid bilayers stained by the potentiometric Di-8-ANEPPS dye. We measure the absolute change in the index of refraction due to the electro-optical effect along a chosen polarization axis. Since lipid bilayers are considered as an adequate model for the investigation of the electric properties of biological membranes (17), electro-optical measurements were subsequently performed on a phosphatidylcholine bilayer built-up on a parylene biochip. Our results demonstrate the imaging capability of an advanced electro-optical microscope in a microfluidic environment suitable for biology-related studies.

PRINCIPLE AND THEORY

The electro-optical (EO) effect of a noncentrosymmetric material, or Pockels effect, is the change of the index of refraction of this medium in response to a quasistatic electrical field applied using adequately-shaped electrodes (18). The change in the index of refraction can be read out as an additional small phase shift on a probing light wave. Although the Pockels effect stems from a second-order (rank three) nonlinearity, it can also be viewed as a linear optical response in the electric field of the probe light field $\vec{E}_{op}$, which also depends linearly on the applied external quasistatic electrical field $\vec{E}_S$.

The change in the index of refraction along the i axis is given by

$$\Delta n_i \approx -\frac{n_i^3}{2}\sum_j r_{ij}E_j, \tag{1}$$

where E_j is the component of the applied electric field $\vec{E}_S$ in the j direction (see Appendix A). The proportionality factors r_{ij} are the coefficients of the electro-optical tensor (18). We choose $\{x,y,z\}$ as the principal axes of the nonlinear material, i.e., z axis is perpendicular to the plane of the doped bilayer (see Fig. 1) along the applied field direction, and x,y are arbitrary directions in the sample plane.

Depending on the orientation of the molecules inside the medium and the associated geometrical symmetry, some r_{ij} coefficients cancel and some are related to one another. In the case of an artificial bilayer doped with an ensemble of dye molecules, the assumed statistical cylindrical symmetry around the z axis leads to the tensor

$$[r_{ij}] = \begin{pmatrix} 0 & 0 & r_{13} \\ 0 & 0 & r_{13} \\ 0 & 0 & r_{33} \\ 0 & r_{13} & 0 \\ r_{13} & 0 & 0 \\ 0 & 0 & 0 \end{pmatrix}. \tag{2}$$

In this notation, index 3 is related to the z direction of propagation of the light, perpendicular to the membrane and supporting substrate (see Fig. 1).

The induced EO phase shift is

$$\Delta\varphi_i = \frac{2\pi}{\lambda}e\Delta n_i, \tag{3}$$

which can be developed into the field-dependent expression

$$\Delta\varphi_i = -\frac{\pi}{\lambda}en_i^3\sum_j r_{ij}E_j. \tag{4}$$

A signature of the effect can be obtained by rotating the polarization of the linearly polarized incident light. Inspection of the electro-optical tensor matrix shows that the phase shift must not change when the polarization of the incident beam is rotated within the (x,y) plane of the sample, as it involves the same r_{13} EO coefficient, in agreement with the cylindrical symmetry about the z axis. We therefore note that a polarimetric detection setup with crossed polarizer and analyzer, which is sensitive to a differential phase shift between two orthogonal directions, would not be able to detect an isotropic phase shift as in this case.

An optical scheme capable of measuring the absolute EO phase shift along one given polarization direction is therefore required. Such a scheme could measure the electrical field $\vec{E}_S$ if the EO coefficients are known, or conversely the EO coefficients can be extracted when the electric field $\vec{E}_S$ is known. If both are undefined, one can then access the $E_j\, r_{ij}$ product.

Assuming a potential of 10 mV throughout a membrane of $e = 7$ nm thickness and a realistic r coefficient of ~1 pm/V for a doped membrane, one should be able to measure a corresponding phase shift variation $\Delta\varphi$ of $\sim 10^{-7}$ rad.

To measure this additional EO dephasing contribution, we use an interferometric scheme described below.

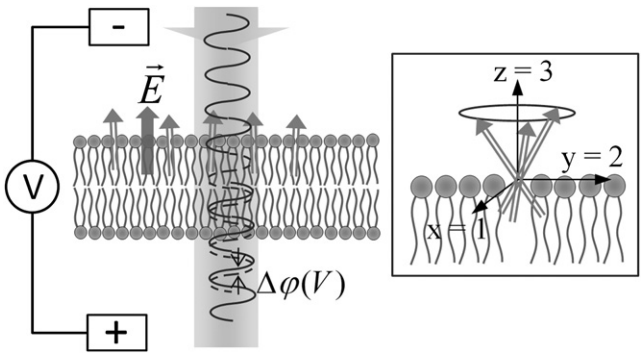

FIGURE 1 Principle of probing the electro-optical effect of a one-side dye-doped membrane. (*Inset*) Orientation distribution of the dye molecules in the upper layer.

SAMPLE AND OPTICAL METHODS

Electro-optic microscope

The principle of measuring an electro-optical phase shift is shown in Fig. 2. A continuous-wave He-Ne laser is used as the light source, its beam being subsequently split in two parts. One part is focused on the doped lipidic membrane through a microscope objective (CFI Plan-Fluor 40×, NA = 0.6; Nikon France S. A. S., Champigny-sur-Marne, France), then transmitted and

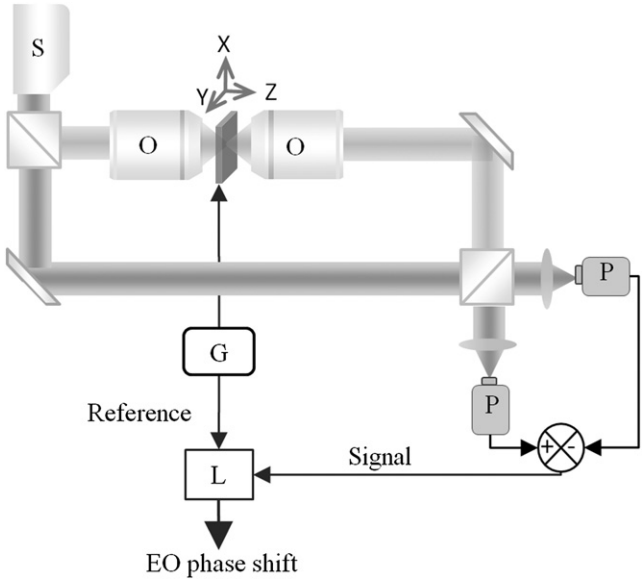

FIGURE 2 Simplified scheme of the interferometric microscope used to detect the electro-optical phase shift associated to the dye-doped membrane. Key: S, continuous-wave HeNe laser source; O, microscope objective (40×, NA 0.6); P, photodiode; G, high-frequency voltage generator; and L, lock-in amplifier.

collected via an identical microscope objective in the forward direction. It is then recombined with the other beam that plays the role of the reference arm in a Mach-Zehnder interferometric scheme (19). The optical interference signal is detected by two photodiodes (Hamamatsu, Hamamatsu City, Japan). The electric field applied on the sample is modulated at a fixed frequency Ω ranging typically from 20 kHz to 100 kHz, inducing a modulated phase shift and interference fringes changes at the same frequency. To reach a high sensitivity for detecting a small phase shift variation, a balanced homodyne detection system based on two photodiodes is being used (20). A lock-in amplifier (Model 5302; EG&G Princeton Applied Research, Oak Ridge, TN) is used to measure this modulated phase shift with high signal/noise ratio. The sensitivity of the interferometric detection to the EO phase shift is maximized if the static optical path difference between the two beams corresponds to a phase shift $\varphi_{LO} = \pi/2$ rad. A phase control loop is therefore implemented in the system, with a mirror mounted on a piezo-electrical transducer stage (PI Ceramic, Lederhose, Germany). It is added to the optical path of the reference beam and its translation allows us to change the quasistatic optical path length (not shown in Fig. 2).

Let us note that in principle an electrically induced absorption modification would also lead to a signal modulated at frequency Ω. However, with the above phase bias point $\varphi_{LO} = \pi/2$ rad, the lock-in amplifier is only sensitive to the EO phase-shift, whereas $\varphi_{LO} = 0$ rad would render the detection system sensitive to a modulated absorption (see Appendix C).

Two half-wave plates (Optique Fichou, Fresnes, France) allow us to control the polarization of the light focused onto the sample.

Sample composition and fabrication

Biochip

As a sample holder, we use a homemade biochip constituted of parylene. It is encapsulated in a resin that has been photopatterned in three dimensions thanks to a stereolithography process (21). The parylene thin film of 20-μm thickness was micromachined using O_2 plasma in reactive-ion-etching through an aluminum mask, which leads to an array of through holes devoted to the bilayer reconstruction. In each microchamber, nine holes of 40-μm diameter allowed the simultaneous formation of nine bilayers (22–24).

Electrodes

Two Ag/AgCl electrodes, connected to the solutions from each side of the bilayer, were used to apply a voltage difference. The coating of silver electrodes is deposited by dipping the electrodes for five minutes in a nitric and hydrochloric acid (1:3 vol/vol) concentrated solution. By dipping the electrodes in this bath for five minutes, we obtained a pure, thin, and uniform chloride silver coating.

Mechanism of bilayer formation

Before this experiment, the biochip is first put into an ultrasound bath in ethanol solution for 5 min, and then in another ultrasound bath in Millipore water solution (Bioblock, Millipore, Molshein, France) for 2 min. It was rinsed with Millipore water, dried with compressed nitrogen, and then further dried in an oven (40°C, 10 min).

Fifteen microliters of a buffer solution of 0.1 M KCl (Thermo Fisher Scientific, loughorough, UK) and 10 mM, pH7 3-(*n*-morpholino)propanesulfonic acid) (MOPS; Research Organics, Cleveland, OH) were inserted in the upper chamber. The lipid used was L-α-phosphatidylcholine (Egg chicken, Avanti Polar Lipids, Alabaster, AL), 20 mg/mL dissolved in *n*-decane (Merck, Hohenbrunn, Germany). Eight microliters of the lipid solution were flowed in the lower channels, followed by the flowing of the buffer, which permits the formation of the bilayers, as described in the literature (21,22).

Staining of the bilayer

To generate an electro-optical phase shift, the medium has to display a noncentrosymmetric statistical arrangement. The lipid molecule by itself satisfies this condition, but in the case of a bilayer, the head-tail molecular assembly leads to a centrosymmetric system, and subsequent cancellation of the EO effect. To confer electro-optical activity to the membrane, we asymmetrically stained the membrane with a noncentrosymmetric probe molecule Di-8-ANEPPS (Invitrogen, Carlsbad, CA). This molecule has a long carbon chain, thus adequately lengthening the flip time across the membrane (9,25). Those properties make Di-8-ANEPPS a dye that has been widely used for fluorescence or SHG measurement of membranes (26,27), and as an electrical potential probe (9,12,25,28–32). Its orientation in the membrane was investigated (27,33), and different models were proposed.

The stock solution was prepared in dimethyl-sulfoxide (DMSO; Sigma Aldrich, St. Louis, MO) at 1 mg/mL concentration. Three microliters of the dye was introduced to the upper chamber already filled with the buffer (see Fig. 3 *a*), and the lipid was injected in the lower channel (see Fig. 3 *b*). A glass plate was then placed on the biochip to cover the upper chamber. It was perforated to insert an electrode inside the buffer solution. The glass plate was used to prevent the formation of a curved liquid surface that could act as a microlens and thus affect the probe laser beam that passes through it. Then, as explained above, the buffer was introduced in the lower channel and the bilayer formed (see Fig. 3 *c*). A 15-min waiting time between the introduction of the dye and the start of the measurement allowed the dye to intercalate into the upper layer of the artificial bilayer.

To check that the lipidic membrane was organized as a bilayer, a capacitance measurement between both sides of the membrane was made before and after the electro-optical measurement described below. The same capacitance 0.32 μF/cm^2 measured at the beginning of the experiment was also found at the end. This is in good agreement with the values of surface capacitance of bilayers (0.4 μF/cm^2) reported in the literature (34).

RESULTS

With the bilayer stained as explained above, we performed the electro-optical measurement. The dye was inserted on one side of the lipidic membrane, and a modulated electric field was applied between both sides of this membrane. A sinusoidally varying potential difference of up to 10 V maximum

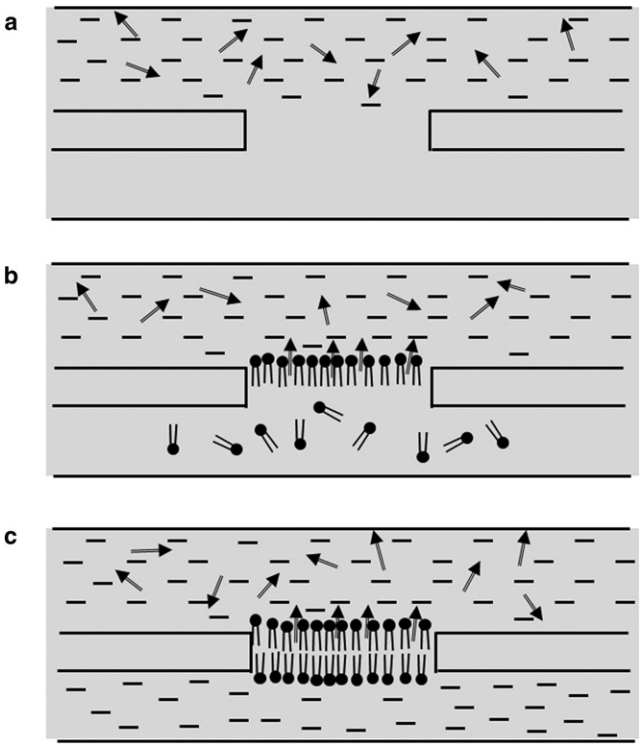

FIGURE 3 Steps of bilayer formation. (*a*) Insertion of the buffer and the dye in the upper channel; (*b*) injection of the lipid in the lower channel; and (*c*) injection of the buffer solution in the lower channel and formation of the bilayer.

amplitude was applied to the membrane without breaking it, and its electro-optical response was recorded.

The modulated electric field induced a modulated phase shift in the laser beam that probes the EO active sample. Although the signal was small, our interferometric setup proved sensitive enough for measuring this electro-optical phase shift through the membrane.

First, the electro-optical signal was detected with a good signal/noise ratio. For a voltage difference of 5 V peak-to-peak amplitude at 100 kHz, the signal/noise ratio was 10 ± 1 for 20-ms integration time. Second, we observed that the temporal response of the system was fluctuating (Fig. 4). This may be due to impurities inside the buffer passing through the probe beam during the measurement.

The frequency of the modulated electric field applied to the membrane is limited by the cutoff frequency of the system. The bilayer and the surrounding buffer can be modeled as a capacitor and a resistance (35). We estimate a cutoff frequency of ~3 MHz, well above the frequency used for the measurement. As for the conductivity of the buffer necessary to transfer the voltage difference to the membrane at a given frequency, we calculated its cutoff frequency to be ~260 MHz.

To check the origin of the detected signal, we changed the amplitude of the applied potential difference. The temporal signal of the lock-in amplifier was recorded for each

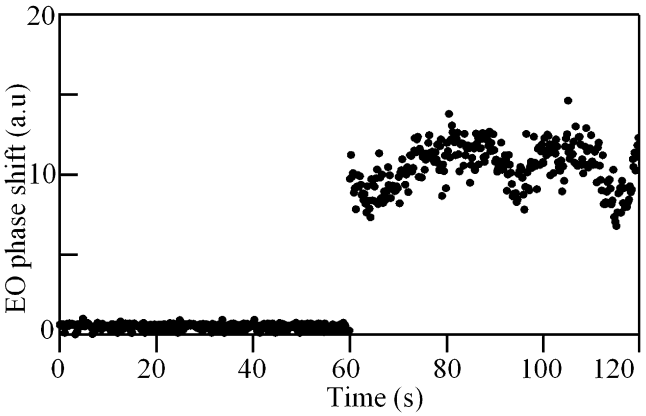

FIGURE 4 Electro-optical temporal response of the bilayer without any modulating field, then while applying a difference of potential of amplitude 5 V modulated at 20 kHz frequency. The signal/noise ratio is ~10 ± 1 for 20-ms integration time.

modulated voltage amplitude, and the dependence of the EO signal on the applied electric field was plotted. We note here that the sensitivity of our system was found to be of 100-mV potential difference amplitude. Fig. 5 shows a linear dependence, as expected for the Pockels effect (from Eq. 1). From the slope of this curve, we could extract the electro-optical coefficient of the membrane. The slope $\Delta\varphi/E$ is $(30.6 \pm 1.2) \times 10^{-5}$ rad.nm/V, which is theoretically equal to $(\pi/\lambda)en^3r_{13}$ (see Eq. 18). The laser wavelength λ is 632.8 nm. It is difficult to give accurate values to the thickness and index of refraction of the membrane for the electro-optical response. Here we make the assumption that a macroscopic description of this ultrathin optical device is valid, which is commonly done for thin films (10). Under this assumption, $e = 7$ nm and $n \approx 1.5$ seem to be safe values, which have been used in the literature (36). Then one can estimate the membrane EO coefficient $r_{13} = 2.6$ pm/V. This value seems reasonable, as it can lead to nonnegligible SHG signals such as those reported in Ries et al. (27).

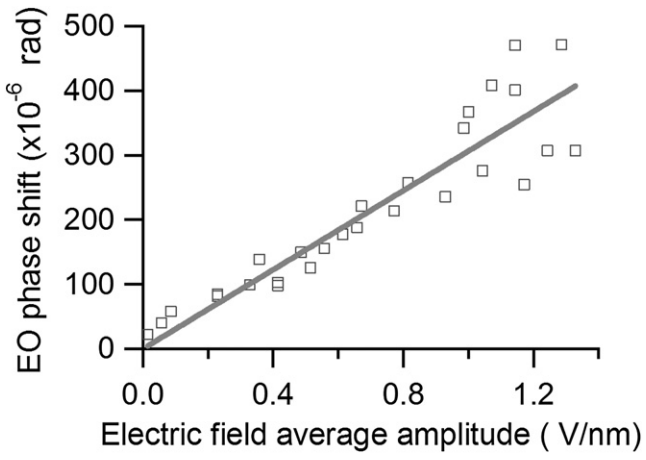

FIGURE 5 EO phase shift versus applied modulated electric field amplitude.

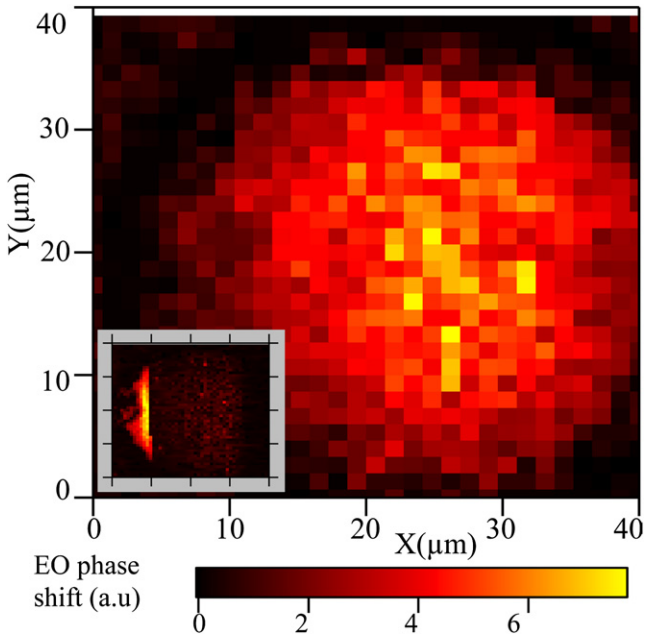

FIGURE 6 Scan image of the EO response of dye-doped bilayer. (*Inset*) Destruction of the bilayer during a scan.

Fig. 6 shows a typical raster scan of a membrane under a 5 V peak-to-peak sinusoidal voltage at 20 kHz frequency. The contour of the hole holding the membrane can be distinguished. The signal is higher at the center of the membrane, perhaps due to a higher density of Di-8-ANEPPS molecules at the center of the hole, itself due to a possible Gibbs plateau on the circumference of the hole. The inset in Fig. 6 shows another scan during which the membrane was broken.

To test the symmetry of the dye orientation distribution, the linear polarization of the incoming light was switched perpendicular to the previous one, i.e., from x to y axis in Fig. 1. The results are given in Table 1. The signal did not change within 2%, as expected from the cylindrical symmetry about the z axis (see Fig. 1), hence the same electro-optical coefficient is found in both configurations. Again, we note that this isotropic phase shift distribution of the EO variation of the index of refraction could not be detected by a standard polarimetric setup that would be only sensitive to birefringence.

TABLE 1 Measured EO phase shifts in radian for two perpendicular light polarizations passing through the sample

	EO phase shift ($\times 10^{-4}$ rad)	
Polarization of the light	Artificial membrane	$LiNbO_3$ crystal
x	2.09 ± 0.14	1.82 ± 0.15
y	2.12 ± 0.23	20.12 ± 2.32

In the case of an artificial membrane, the EO phase shift is the same for both polarizations (5 V at 20 kHz) within error, and in the case of a reference sample made of a $LiNbO_3$ crystalline plate, the ratio between the two signals is ~10 (modulation of 10 V at 20 kHz).

We compared such a response to a homemade reference sample built with a $LiNbO_3$ single crystal plate (see Table 1). This reference is highly anisotropic in its x and y EO responses, which confirmed the polarization sensitivity of our interferometric detection method. Therefore, any change of dye alignment in the membrane can be readily detected by our setup.

DISCUSSION AND CONCLUSION

In this article, we demonstrated that the electro-optical effect can be used to quantitatively image a dye-doped artificial membrane. We checked that the EO response is proportional to the applied voltage difference as expected for the Pockels effect. Using different optical polarizations, we also checked the symmetry of the doped membrane around the direction normal to the bilayer, and proved that this microscopy is able to probe the statistical orientational order of the dye inside the membrane. We point out that this interferometer is sensitive to electro-optical variations of the index of refraction along any given polarization direction. Estimating the applied electrical field, we obtained a reasonable value for the dye-doped membrane nonlinear susceptibility $r_{13} \approx 2.6$ pm/V. If the nonlinear susceptibility is known independently, for instance from a SHG measurement, our method provides a nonresonant optical measurement of the transmembrane potential. This second approach therefore allows the investigation of electrical fields in doped lipid membranes.

We note that the above results rely on average values over the membrane. A future analysis taking into account the distribution of the field and exact molecular insertion could be performed by using different dye molecules. At the scale of a single layer of molecules, we may also observe heterogenous physical effects, in terms of thin-film organization and for multicomponent membranes, which will require a refined model.

We note that a modulated sinusoidal potential difference of 1 V amplitude at a relatively high frequency, varied from 20 to 100 kHz, was not invasive to the membrane. For an unstained membrane the voltage reached 4 volts peak to peak at frequency = 20 kHz before breaking the membrane, in the case of an electrical capacitance of 33 pF for nine simultaneous bilayers. With stained lipidic membranes, some of them could withstand an applied voltage of up to 20 volts peak to peak at 20 kHz, without damage. This observation is quite surprising, as it is well known that when a DC potential difference higher than 1 V is applied to a bilayer, it is depolarized by the corresponding static electric field and the membrane is broken (37–39). The enhanced robustness of the membrane to higher voltages is probably linked to the sinusoidal character of the potential difference. This unexpected result has to be investigated in future work.

Although our electrical measurements and separate optical observations of the Gibbs ring under a regular

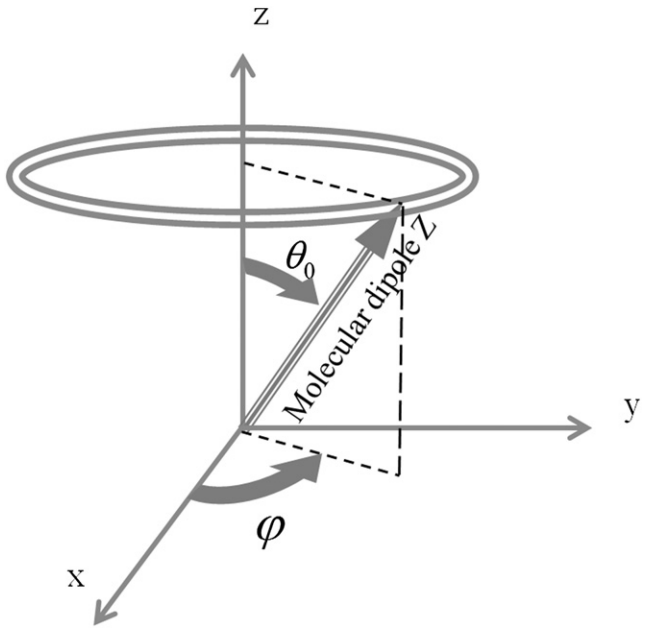

FIGURE 7 Molecule orientation with respect to the coordinate axes.

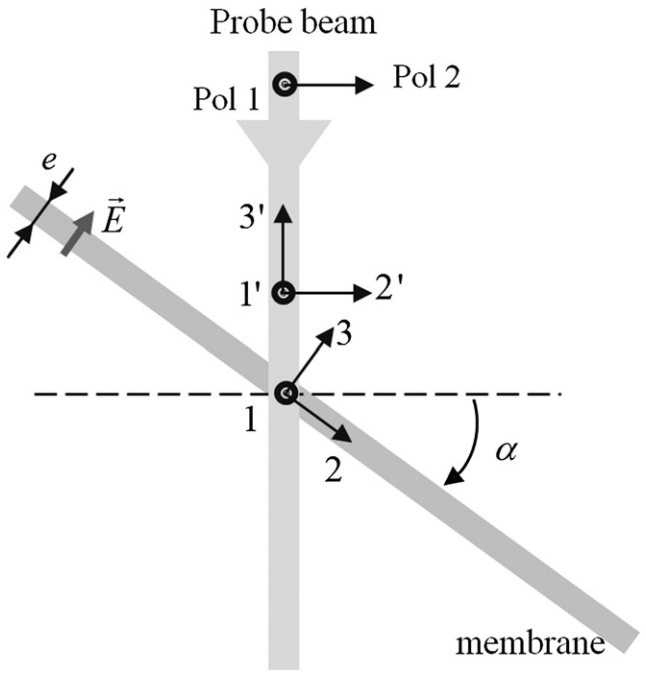

FIGURE 8 Scheme of axes configuration in the case of a tilted membrane.

microscope support the existence of a thin bilayer in our biochip, we note that the robustness of the film to high voltage difference would be possible for a thicker film. We also note that the conclusions raised here concerning electro-optical microscopy for a thin film could be applicable to a thick one.

Many developments of the technique can now be envisioned. For instance, to fully characterize the orientational order of the dye in the artificial bilayer (see Fig. 7), with the average tilt angle $\langle\theta_0\rangle$ of a molecule being given by the coefficient ratio $r_{13}/r_{33} = \langle\tan(\theta_0)\rangle/2$ (see Eq. 15), a light polarization in the z axis direction could be applied on the membrane by focusing an inhomogeneously polarized beam (40). Furthermore, new biochips with in flow changing of the buffer solution in the upper chamber can also be designed. It would allow us to change the dye concentration during a single experimental measurement, insert membrane proteins or membrane ion channels, and add inhibitors or activators of these proteins.

Finally, we can also envision probing the depolarization of a plasma membrane after stimulation and in the long-term, the propagation of an action potential in an excitable cell. However, some bottlenecks have to be considered. Firstly, such an internally generated electrical field is a self-triggered train of pulses rather than a sine wave at a definite frequency. Therefore, a new asynchronous detection technique has to be developed. The pulse repetition rate being also low, an heterodyne detection would be a good candidate to shift low frequency to a higher noiseless one (41). Secondly, in the case of a living cell the surface is not flat, thus leading to a tilt angle α of the normal direction to the membrane, with respect to the microscope z axis at the probe beam position (see Fig. 8). In this case, new electro-optical coefficients will appear (see Eq. 22). A simultaneous polarization measurement in two perpendicular polarizations could measure this local tilt α . Near the border of the cell, we expect an increase of sensitivity. The electric field is aligned with the dye molecules and the polarization of the probe beam. The $r_{33} = 2.5r_{13}$ will be probed, increasing the sensitivity 2.5 times. Thirdly, to increase our sensitivity, the intensity of the probe beam can be increased while enlarging the diameter of the focused beam to keep any photobleaching at a constant level. Therefore, the sensitivity could be increased at the cost of the focused probe beam size. Fourthly, for thick biological samples the transmission mode is clearly a limitation. A reflective configuration could be used because the index of refraction variation under an applied electric field induces a variation of the reflection coefficient of the membrane. Using Abeles matrix in a stratified media (19), the expected intensity reflection coefficient is $\sim 10^{-5}$ in intensity, and the electro-optical contribution is estimated to be $\approx 2 \times 10^{-8}$. A modified setup with enhanced sensitivity is envisioned to detect this small effect. Finally, it could be interesting to couple two-beam interferometric technique with polarimetry in transmission (42), or total internal reflection geometry (43).

Although the goal of applying our technique to the electrical activity of a living cell, currently under investigation in our lab, remains challenging, the results presented here sound prerequisite toward further exploration of an all-optical patch-clamp technique.

APPENDIX A: RELATION BETWEEN THE NONLINEAR SUSCEPTIBILITY AND MOLECULAR ORIENTATION

The electro-optical (EO) effect is the change of the refractive index of a medium in response to a quasistatic electrical field. This effect is related to the second-order nonlinearity and the related EO susceptibility is given by

$$\chi^{(2)}_{ijk}(\omega + \Omega;\omega,\Omega) = Nf^2(\omega)f(\Omega)\iint \beta_{ijk}(\omega + \Omega;\omega,\Omega)P(\breve{\rho})d\breve{\rho}, \quad (5)$$

where $\chi^{(2)}_{ijk}(\omega+\Omega;\omega,\Omega)$ is the nonlinear second-order susceptibility, ω is the optical frequency, and Ω is the applied electrical field frequency, which can be assumed quasistatic compared to that of the optical frequency. The value N is the density of nonlinear chromophores, β is their molecular hyperpolarizability, and $\breve{\rho}$ is the solid angle related to the orientation of the molecules, as defined for each molecule by its set of Euler angles. The values $f(\omega)$ and $f(\Omega)$are the local field factors at the optical frequency and quasistatic frequency, respectively. Referring to x,y,z laboratory frame, i,j,k are the macroscopic coordinates. The β-tensor of the molecule is known and simple in the axes X,Y,Z associated to the geometry of the molecule. It can be assumed to be one-dimensional and having one nonzero component β_{zzz}. This is in agreement with the quasi-one-dimensional structure of the dye and related intramolecular charge transfer that underlies the β-tensor. The associated coordinates are I,J,K. Taking into account the transformation from X,Y,Z to x,y,z for laboratory axes, Eq. 5 becomes

$$\chi^{(2)}_{ijk}(\omega + \Omega;\omega,\Omega) = Nf^2(\omega)f(\Omega) \times \sum_{IJK}\iint \beta_{IJK}(\omega + \Omega;\omega,\Omega)P(\breve{\rho})(\hat{I}.\hat{i})(\hat{J}.\hat{j})(\hat{K}.\hat{k})d\breve{\rho}. \quad (6)$$

In the case of a bilayer having a thickness e, doped by a nonlinear dye with a surface density N_s, we have $N = N_s/e$.

We assume that the molecules are oriented inside the membrane in a cone with a symmetry around the normal z to the membrane surface as shown in Fig. 1 and Fig. 7, θ_0 being the angle of this cone with respect to the normal direction.

In the case of a dye oriented inside a membrane in first approximation, one can express the probability of orientation as $P(\breve{\rho}) = \delta(\theta-\theta_0)/2\pi\sin\theta_0$, therefore

$$\chi^{(2)}_{ijk}(\omega + \Omega;\omega,\Omega) = \frac{N_s}{e}f^2(\omega)f(\Omega)\beta_{ZZZ}\frac{\iint \delta(\theta-\theta_0)(\hat{I}.\hat{i})(\hat{J}.\hat{j})(\hat{K}.\hat{k})d\theta d\varphi}{2\pi}. \quad (7)$$

This cylindrical symmetry leaves only two independent nonzero coefficients of the $\chi^{(2)}$ tensor, namely

$$\chi^{(2)}_{zzz} \text{ and } \chi^{(2)}_{xxz} = \chi^{(2)}_{yyz} = \chi^{(2)}_{yxy} = \chi^{(2)}_{xzx}, \quad (8)$$

with

$$\chi^{(2)}_{zzz} = \frac{N_S}{e}f^2(\omega)f(\Omega)\beta_{ZZZ}\cos^3\theta_0 \quad (9)$$

and

$$\chi^{(2)}_{xxz} = \frac{N_S}{e}f^2(\omega)f(\Omega)\beta_{ZZZ}\frac{\sin^2\theta_0\cos\theta_0}{2}. \quad (10)$$

Electro-optic coefficients

The electro-optical coefficients are related to the second-order susceptibility (44), by the relation

$$r_{ijk}(\omega) = -\frac{2\chi^{(2)}_{ijk}\left(\omega + \Omega;\omega,\Omega\right)}{n^2_{ii}n^2_{jj}}. \quad (11)$$

We can write those coefficients in the contracted indices mode where ijk will become lk and l stands for a combination of ij (45). It follows Table 2. From the above geometry and dye characteristics, the electro-optical coefficient tensor matrix of our doped artificial bilayer takes the form

$$\left[r_{lj}\right] = \begin{pmatrix} 0 & 0 & r_{13} \\ 0 & 0 & r_{13} \\ 0 & 0 & r_{33} \\ 0 & r_{13} & 0 \\ r_{13} & 0 & 0 \\ 0 & 0 & 0 \end{pmatrix}, \quad (12)$$

where

$$r_{13} = -\frac{N_s}{en^4}f^2(\omega)f(\Omega)\beta_{ZZZ}\sin^2\theta_0\cos\theta_0 \quad (13)$$

and

$$r_{33} = -\frac{N_s}{en^4}f^2(\omega)f(\Omega)\beta_{ZZZ}2\cos^3\theta_0, \quad (14)$$

taking $n \approx n_{ii} \approx n_{jj}$.

These expressions show the dependence of the electro-optical coefficient on the orientation angle θ_0 of the dye. The ratio between the two coefficients is directly linked to this angle:

$$\frac{r_{13}}{r_{33}} = \frac{\tan(\theta_0)}{2}. \quad (15)$$

EO-induced phase shift

The additional EO phase shift across a membrane of thickness e, when the beam is polarized along the $\hat{i}$ direction, can be expressed as

$$\Delta\varphi_i = \frac{2\pi}{\lambda}e\Delta n_i, \quad (16)$$

so that

$$\Delta\varphi_i = \frac{-\pi}{\lambda}en_i^3\sum_j r_{ij}E_j, \quad (17)$$

where E_j is the applied quasistatic electric field.

In the configuration where the applied electric field is in the direction normal to the membrane, i.e., along z, the only nonzero component of the electrical field is E_3, then

$$\Delta\varphi_1 = \frac{-\pi}{\lambda}en^3r_{13}E_3, \quad (18)$$

TABLE 2 Contracted indices

ij	$xx=11$	$yy=22$	$zz=33$	$yz=23$	$xz=13$	$xy=12$
l	1	2	3	4	5	6

$$\Delta\varphi_2 = \frac{-\pi}{\lambda} en^3 r_{13} E_3, \tag{19}$$

$$\Delta\varphi_3 = \frac{-\pi}{\lambda} en^3 r_{33} E_3. \tag{20}$$

APPENDIX B: THE CASE OF A BIOLOGICAL MEMBRANE

In the case of a cell membrane, the surface is not horizontal and the morphology can be more complex. The simplest model is that of a bilayer with a tilt angle α with respect to the horizontal line (see Fig. 8).

In this configuration the new electro-optical coefficients, as read in the principal axis frame (1′,2′,3′), can be expressed as a function of the coefficients in the membrane axis local frame (1–3). They can be written via classical tensor relations

$$r_{i',j',k'} = \sum_{i,j,k} r_{i,j,k}\left(i,i'\right)\left(j,j'\right)\left(k,k'\right). \tag{21}$$

In the new axis system, the EO coefficient tensor will then be given by

$$\left[r_{l'j'}\right] = \begin{pmatrix} 0 & r_{13}\sin\alpha & r_{13}\cos\alpha \\ 0 & 3r_{13}\cos^2\alpha\sin\alpha + r_{33}\sin^3\alpha & r_{13}\left(3\cos^3\alpha - 2\cos\alpha\right) + r_{33}\sin^2\alpha\cos\alpha \\ 0 & r_{13}\left(\sin^3\alpha - 2\cos^2\alpha\sin\alpha\right) + r_{33}\cos^2\alpha\sin\alpha & 3r_{13}\sin^2\alpha\cos\alpha + r_{33}\cos^3\alpha \\ 0 & r_{13}\left(\cos^3\alpha - 2\sin^2\alpha\cos\alpha\right) + r_{33}\sin^2\alpha\cos\alpha & r_{13}\left(\sin^3\alpha - 2\cos^2\alpha\sin\alpha\right) + r_{33}\cos^2\alpha\sin\alpha \\ r_{13}\cos\alpha & 0 & 0 \\ r_{13}\sin\alpha & 0 & 0 \end{pmatrix}. \tag{22}$$

The new phase shift under two perpendicular polarizations can be expressed as

$$\Delta\varphi_{1'} = \frac{\pi N_s f^2(\omega) f^2(\Omega)\beta_{ZZZ}}{\lambda\, en^7} \frac{\sin^2\theta_0\cos\theta_0}{\cos\alpha} V, \tag{23}$$

$$\Delta\varphi_{2'} = \frac{\pi N_s f^2(\omega) f^2(\Omega)\beta_{ZZZ}}{\lambda \quad en^7} \times \frac{\cos^2\alpha\sin^2\theta_0\cos\theta_0 + 2\cos^3\theta_0\sin^2\alpha}{\cos\alpha} V. \tag{24}$$

A dependency on the tilt angle α is clearly expected.

APPENDIX C: HOMODYNE AND SYNCHRONOUS DETECTION

If a reference beam of amplitude $\overline{\alpha}_{LO}$ is interfering with a signal beam of amplitude $\overline{\alpha}_S$, the difference in the intensities detected by the two photodiodes used in balanced homodyne detection configuration is

$$\Delta I = 2\overline{\alpha}_{LO}\overline{\alpha}_S\cos(\Delta\varphi - \varphi_{LO}), \tag{25}$$

where φ_{LO} is the static optical phase-shift between the two beams paths, and $\Delta\varphi$ is the electro-optical phase-shift in the signal path. Although we are interested in measuring $\Delta\varphi$, one can wonder whether a signal amplitude variation due to absorption or emission $\Delta\overline{\alpha}_S$ could contribute to the signal.

Two regimes are of interest depending on the static phase shift value.

Firstly, if $\varphi_{LO} = \pi/2$ rad, Eq. 25 became $\Delta I = 2\overline{\alpha}_{LO}\overline{\alpha}_S\cos\Delta\varphi$, provided that the electro-optical phase shift $\Delta\varphi$ is small. The electric field being modulated at a frequency Ω, the EO phase shift will be modulated at the same frequency ($\Delta\varphi = \varphi_0\cos(\Omega t + \theta_1)$) as well as the emission or absorption: $\overline{\alpha}_S = \overline{\alpha}_S + \Delta\overline{\alpha}_S(\Omega) = \overline{\alpha}_S + \overline{\alpha}_{S_0}\cos(\Omega t + \theta_2)$. Then

$$\Delta I = 2\overline{\alpha}_{LO}\overline{\alpha}_S\varphi_0\cos(\Omega t + \theta_1) + \overline{\alpha}_{LO}\overline{\alpha}_{S0}\varphi_0(\cos(\theta_1 - \theta_2) + \cos(2\Omega t + \theta_1 + \theta_2)). \tag{26}$$

The synchronous detection multiplies ΔI by a reference signal at the electric field frequency Ω. After such a multiplication, the DC component carries the information of the EO phase shift corresponding to the first term in Eq. 26, $\overline{\alpha}_{LO}\overline{\alpha}_S\varphi_0$. The two last components are shifted spectrally to higher frequencies Ω and 3Ω, which includes the intensity variation $\Delta\overline{\alpha}_S$ due to absorption or emission variation. Therefore, $\Delta\overline{\alpha}_S$ will not show up in the final detected DC signal.

Secondly, if $\varphi_{LO} = 0$, the intensity difference then becomes $\Delta I = 2\overline{\alpha}_{LO}\overline{\alpha}_S\cos(\Delta\varphi) \approx 2\overline{\alpha}_{LO}\overline{\alpha}_S$, if $\Delta\varphi$ is very small. In this case, any variation in the amplitude of the signal due to absorption or emission induced by electric field and modulated with the same frequency will be measured with the lock-in amplifier.

Therefore, an interesting feature of our method is to be able to access either EO coefficients or electric field-induced absorption and emission variations, depending on the phase shift φ_{LO} that we impose between the two interfering beams.

We thank Jean-Pierre Lefèvre and Jean-Pierre Madrange for technical assistance.

We acknowledge contract CNano Microscopie Electro-Optique et Applications and FI Bioimaging. B.H. thanks Centre National de la Recherche Scientifique for the PhD grant. L.H. and T.O. recognize Centre National de la Recherche Scientifique for their postdoctoral grant. H.M. acknowledges a postdoctoral grant from Région Ile-De-France.

REFERENCES

1. Hodgkin, A. L., and A. F. Huxley. 1939. Action potentials recorded from inside a nerve fiber. *Nature*. 144:710–711.
2. Llinas, R., and M. Sugimori. 1980. Electrophysiological properties of in vitro Purkinje cell somata in mammalian cerebellar slices. *J. Physiol.* 305:171–195.
3. Sakmann, B., and E. Neker. 1984. Patch clamp techniques for studying ionic channels in excitable-membranes. *Annu. Rev. Physiol.* 46: 455–472.
4. Cohen, L. B., R. D. Keynes, and B. Hille. 1968. Light scattering and birefringence changes during nerve activity. *Nature*. 218:438–441.
5. Cohen, L. B., B. Hille, and R. D. Keynes. 1970. Changes in axon birefringence during the action potential. *J. Physiol.* 211:495–515.
6. Gupta, R. K., B. M. Salzberg, A. Grinvald, L. B. Cohen, K. Kamino, et al. 1981. Improvements in optical methods for measuring rapid changes in membrane potential. *J. Membr. Biol.* 58:123–137.
7. Cohen, L. B., B. M. Salzberg, and A. Grinvald. 1978. Optical methods for monitoring neuron activity. *Annu. Rev. Neurosci.* 1:171–182.

8. Ross, W. N., B. M. Salzberg, L. B. Cohen, A. Grinvald, H. V. Davila, et al. 1977. Changes in absorption, fluorescence, dichroism, and birefringence in stained giant axons: optical measurement of membrane potential. *J. Membr. Biol.* 33:141–183.
9. Loew, L. M. 1996. Potentiometric dyes: imaging electrical activity of cell membranes. *Pure Appl. Chem.* 68:1405–1409.
10. Zochowski, M., M. Wachowiak, C. X. Falk, L. B. Cohen, Y. W. Lam, et al. 2000. Imaging membrane potential with voltage-sensitive dyes. *Biol. Bull.* 198:1–21.
11. Zecevic, D. 1996. Multiple spike-initiation zones in single neurons revealed by voltage-sensitive dyes. *Nature*. 381:322–325.
12. Gross, E., R. S. Bedlack, and L. M. Loew. 1994. Dual-wavelength ratiometric fluorescence measurement of the membrane dipole potential. *Biophys. J.* 67:208–216.
13. Dombeck, D. A., M. Blanchard-Desce, and W. W. Webb. 2004. Optical recording of action potentials with second-harmonic generation microscopy. *J. Neurosci.* 24:999–1003.
14. Bouevitch, O., A. Lewis, I. Pinevsky, J. P. Wuskell, and L. M. Loew. 1993. Probing membrane-potential with nonlinear optics. *Biophys. J.* 65:672–679.
15. Moreaux, L., T. Pons, V. Dambrin, M. Blanchard-Desce, and J. Mertz. 2003. Electro-optic response of second-harmonic generation membrane potential sensors. *Opt. Lett.* 28:625–627.
16. Toury, T., S. Brasselet, and J. Zyss. 2006. Electro-optical microscopy: mapping nonlinear polymer films with micrometric resolution. *Opt. Lett.* 31:1468–1470.
17. Pons, T., L. Moreaux, O. Mongin, M. Blanchard-Desce, and J. Mertz. 2003. Mechanisms of membrane potential sensing with second-harmonic generation microscopy. *J. Biomed. Opt.* 8:428–431.
18. Boyd, R. W. 2008. Nonlinear Optics. Academic Press, Boston, MA, and Amsterdam.
19. Born, M., and E. Wolf. 1999. Principles of Optics: Electromagnetic Theory of Propagation, Interference and Diffraction of Light. Cambridge University Press, Cambridge, UK.
20. Le Xuan, L., S. Brasselet, F. Treussart, J. F. Roch, F. Marquier, et al. 2006. Balanced homodyne detection of second-harmonic generation from isolated subwavelength emitters. *Appl. Phys. Lett.* 89: 121118.
21. Suzuki, H., B. Le Pioufle, and S. Takeuhci. 2008. Ninety-six-well planar lipid bilayer chip for ion channel recording fabricated by hybrid stereolithography. *Biomed. Microdevices*. 11:17–22.
22. Le Pioufle, B., H. Suzuki, K. V. Tabata, H. Noji, and S. Takeuchi. 2008. Lipid bilayer microarray for parallel recording of transmembrane ion currents. *Anal. Chem.* 80:328–332.
23. Suzuki, H., K. V. Tabata, H. Noji, and S. Takeuchi. 2006. Highly reproducible method of planar lipid bilayer reconstitution in polymethyl methacrylate microfluidic chip. *Langmuir*. 22:1937–1942.
24. Ide, T., and T. Ichikawa. 2005. A novel method for artificial lipid-bilayer formation. *Biosens. Bioelectron.* 21:672–677.
25. Rohr, S., and B. M. Salzberg. 1994. Multiple-site optical-recording of transmembrane voltage (MSORTV) in patterned growth heart cell-cultures—assessing electrical behavior, with microsecond resolution, on a cellular and subcellular scale. *Biophys. J.* 67:1301–1315.
26. Bullen, A., and P. Saggau. 1999. High-speed, random-access fluorescence microscopy: II. Fast quantitative measurements with voltage-sensitive dyes. *Biophys. J.* 76:2272–2287.
27. Ries, R. S., H. Choi, R. Blunck, F. Bezanilla, and J. R. Heath. 2004. Black lipid membranes: visualizing the structure, dynamics, and substrate dependence of membranes. *J. Phys. Chem. B*. 108:16040–16049.
28. Antic, S., and D. Zecevic. 1995. Optical signals from neurons with internally applied voltage-sensitive dyes. *J. Neurosci.* 15:1392–1405.
29. Clarke, R. J. 1997. Effect of lipid structure on the dipole potential of phosphatidylcholine bilayers. *Biochim. Biophys. Acta Biomembr.* 1327:269–278.
30. Clarke, R. J., and D. J. Kane. 1997. Optical detection of membrane dipole potential: avoidance of fluidity and dye-induced effects. *Biochim. Biophys. Acta Biomembr.* 1323:223–239.
31. Shynkar, V. V., A. S. Klymchenko, G. Duportail, A. P. Demchenko, and Y. Mely. 2005. Two-color fluorescent probes for imaging the dipole potential of cell plasma membranes. *Biochim. Biophys. Acta Biomembr.* 1712:128–136.
32. Zhang, J., R. M. Davidson, M. D. Wei, and L. M. Loew. 1998. Membrane electric properties by combined patch clamp and fluorescence ratio imaging in single neurons. *Biophys. J.* 74:48–53.
33. Lambacher, A., and P. Fromherz. 2001. Orientation of hemicyanine dye in lipid membrane measured by fluorescence interferometry on a silicon chip. *J. Phys. Chem. B*. 105:343–346.
34. Fujiwara, H., M. Fujihara, and T. Ishiwata. 2003. Dynamics of the spontaneous formation of a planar phospholipid bilayer: a new approach by simultaneous electrical and optical measurements. *J. Chem. Phys.* 119:6768–6775.
35. Hall, J. E. 1975. Access resistance of a small circular pore. *J. Gen. Physiol.* 66:531–532.
36. Lis, L. J., M. McAlister, N. Fuller, R. P. Rand, and V. A. Parsegian. 1982. Interactions between neutral phospholipid-bilayer membranes. *Biophys. J.* 37:657–665.
37. Crowley, J. M. 1973. Electrical breakdown of biomolecular lipid-membranes as an electromechanical instability. *Biophys. J.* 13:711–724.
38. Kramar, P., D. Miklavcic, and A. M. Lebar. 2007. Determination of the lipid bilayer breakdown voltage by means of linear rising signal. *Bioelectrochemistry*. 70:23–27.
39. Lebar, A. M., G. C. Troiano, L. Tung, and D. Miklavcic. 2002. Interpulse interval between rectangular voltage pulses affects electroporation threshold of artificial lipid bilayers. *IEEE Trans. Nanobioscience*. 1:116–120.
40. Dorn, R., S. Quabis, and G. Leuchs. 2003. Sharper focus for a radially polarized light beam. *Phys. Rev. Lett.* 91:233901.
41. Agrawal, G. P. 1997. Fiber-Optic Communication Systems. Chichester-Wiley, New York.
42. Ropars, G., D. Chauvat, A. Le Floch, M. N. O'Sullivan-Hale, and R. W. Boyd. 2006. Dynamics of gravity-induced gradients in soap film thicknesses. *Appl. Phys. Lett.* 88:234104.
43. Sund, S. E., J. A. Swanson, and D. Axelrod. 1999. Cell membrane orientation visualized by polarized total internal reflection fluorescence. *Biophys. J.* 77:2266–2283.
44. Sigelle, M., and R. Hierle. 1981. Determination of the electrooptic coefficients of 3-methyl 4-nitropyridine 1-oxide by an interferometric phase-modulation technique. *J. Appl. Phys.* 52:4199–4204.
45. Yariv, A., and P. Yeh. 2003. Optical Waves in Crystals—Propagation and Control of Laser Radiation. Wiley, New York.